

pubs.acs.org/JPCL Letter

Computational and Spectroscopic Characterization of the Photocycle of an Artificial Rhodopsin

Madushanka Manathunga, Adam J. Jenkins, Yoelvis Orozco-Gonzalez, Alireza Ghanbarpour, Babak Borhan,* James H. Geiger,* Delmar S. Larsen,* and Massimo Olivucci*



Cite This: J. Phys. Chem. Lett. 2020, 11, 4245–4252



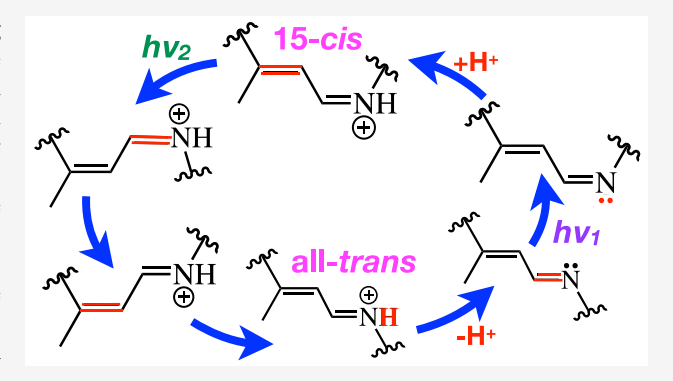
ACCESS

Metrics & More

Article Recommendations

Supporting Information

ABSTRACT: The photocycle of a reversible photoisomerizing rhodopsin mimic (M2) is investigated. This system, based on the cellular retinoic acid binding protein, is structurally different from natural rhodopsin systems, but exhibits a similar isomerization upon light irradiation. More specifically, M2 displays a 15-cis to all-trans conversion of retinal protonated Schiff base (rPSB) and all-trans to 15-cis isomerization of unprotonated Schiff base (rUSB). Here we use hybrid quantum mechanics/molecular mechanics (QM/MM) tools coupled with transient absorption and cryokinetic UV—vis spectroscopies to investigate these isomerization processes. The results suggest that primary rPSB photoisomerization of M2 occurs around the C13=C14 double bond within 2 ps following an aborted-bicycle pedal (ABP) isomerization mechanism similar to



natural microbial rhodopsins. The rUSB isomerization is much slower and occurs within 48 ps around the C15=N double bond. Our findings reveal the possibility to engineer naturally occurring mechanistic features into artificial rhodopsins and also constitute a step toward understanding the photoisomerization of UV pigments. We conclude by reinforcing the idea that the presence of the retinal chromophore inside a tight protein cavity is not mandatory to exhibit ABP mechanism.

Rhodopsins are a family of photoreceptor proteins found in all domains of life. 1-3 All members of the rhodopsin family exhibit a similar protein architecture consisting of a retinal chromophore (a retinal unprotonated (rUSB) or protonated Schiff base (rPSB)) located in a tight protein cavity formed by seven interconnected transmembrane α helices. In the presence of light, rPSB undergoes a selective cis \rightarrow trans or trans \rightarrow cis double bond isomerization initiating crucial biological functions such as visual and nonvisual functions in superior animals, ion transport, ion gating, phototaxis, and gene expression in archea and eubacteria. The rPSB photoisomerization is one of the fastest and most efficient reactions in nature. For instance, in the dim-light visual pigment rhodopsin the isomerization is complete within 200 fs^{4,5} with a 0.65 quantum yield.⁶ The rPSB isomerization in rhodopsin occurs inside a tight protein cavity through a unique space-saving mechanism called aborted-bicycle pedal (ABP) isomerization where two neighboring double bonds isomerize concertedly in opposite directions and one bond completes the isomerization and reaches the product while the other returns to the original configuration.

Recently, Geiger, Borhan and co-workers engineered the first artificial rhodopsin mimics that can reversibly photoisomerize. A hexamutant (R111 K:Y134F:T54 V:R132Q: P39Y:R59Y) of a cytoplasmic protein called cellular retinoic acid binding protein II (CRABPII) (M2) was prepared by

mutating CRABPII such that retinal reacts with a specific lysine residue inside the protein cavity to form a Schiff base linkage and react to light in a way similar to natural rhodopsins. 12-14 Remarkably, M2 appears to display a photochromic cycle (from now on called photocycle) also observed in certain natural rhodopsins (e.g., in Anabaena sensory rhodopsin or in, so-called, bistable rhodopsins such as melanopsin and jumping spider rhodopsin), 15-17 which has been investigated by using UV spectroscopy and X-ray crystallography. In the thermodynamically favored form of M2 (M2_{AT}-USB), the bound chromophore has the all-trans rUSB conformation. When irradiated with UV light (~360 nm), the chromophore isomerizes to the 15-cis rPSB conformation, yielding a new protein form (M2_{15C}-PSB). In the presence of green light (~550 nm) or heat, M2_{15C}-PSB is transformed back to M2_{AT}-USB. Such transformations can be repeated continuously, switching the system between the M2_{AT}-USB and M2_{15C}-PSB forms.

Received: March 9, 2020 Accepted: May 6, 2020 Published: May 6, 2020



The molecular-level elucidation of the intermediate steps driving the M2 photocycle appears to be an important endeavor. This is key in identifying engineering rules allowing for the design and preparation of artificial light-responsive proteins mimicking natural systems. These can provide new molecular devices ^{18–21} functioning as sensors and actuators useful in bioimaging and neuromedical science and, more generally, in synthetic biology. ²²

Due to the current absence of spectroscopic and theoretical studies, our present knowledge of the steps driving the M2 photocycles are, regrettably, highly incomplete. To date, only a single dynamic study on a triple mutant of CRABP-II has been reported.²³ In the present work we are particularly interested in the direct (*all-trans* to 15-*cis*) and reverse (15-*cis* to *all-trans*) photochemical steps. Indeed, (i) such photochemical steps have not been characterized in several aspects such as isomerization mechanism and time scale and (ii) the following thermal steps, corresponding to successive conformational changes and connecting M2_{AT}-USB to M2_{15C}-PSB and *vice versa* has also not been resolved.

The current information on M2 reveals several biomimetic features. In fact, (i) while the CRABPII is very different from opsin, the retinal chromophore isomerizes upon irradiation and it is somehow coupled with proton translocation as in certain microbial rhodopsins;³ however, (ii) the isomerization takes place around C15=N rather than the C11=C12 or C13=C14 bonds of natural rhodopsins. Thus, the investigation of the M2 photocycle will not only allow us to uncover the missing information mentioned above, but will also provide a model for studying how the protein/chromophore interactions affect the rhodopsin photoisomerization regioselectivity in general.

To address the issues above, we have used a combined computational and experimental approach. More specifically, we use a subpopulation of 20 initial conditions to simulate the light induced dynamics of M2_{15C}-PSB and M2_{AT}-USB for up to 0.8 ps via Tully's semiclassical trajectory computations at the state average CASSCF/6-31G*/AMBER level of theory (see section SI1).²⁴ The construction of QM/MM models of both M2_{1SC}-PSB and M2_{AT}-USB is performed by using recently reported ASEC-FEG protocol²⁵ that involves geometry optimization on a free energy, rather than potential energy, surface. Such models are subsequently used to study the reaction time scales using semiclassical trajectories. In addition to the trajectories, the possible reaction paths for M2_{AT}-USB photoisomerization around C11=C12, C13=C14, and C15=N bonds are mapped by using relaxed scans. The results of simulations are compared against time-resolved and temperature resolved dynamics. The sample preparation and experimental protocols are outlined in section S2. Ultrafast transient broadband absorption spectroscopy was performed at room temperature as previously described²⁶ to ascertain the efficiency of these photoreactions. The M2_{15C}-PSB and M2_{15C}-PSB photodynamics were initiated with 565 and 400 nm, respectively. Temperature and time-resolved dynamics were measured by using cryokinetic UV-vis absorption spectroscopy as previously reported and outlined in the Supporting Information.²⁷ LEDs resonant with absorption bands of the starting populations were used to initiate the photoreaction, and the cryogenic temperatures trap the resulting photointermediates. As the temperature of the sample is raised, the photointermediates evolve, allowing for the mapping of the photomechanism.

 $M2_{15C}$ -PSB and $M2_{AT}$ -USB QM/MM Models. The wavelength of the absorption maximum ($\lambda_{\rm max}$) of $M2_{15C}$ -PSB and $M2_{AT}$ -USB computed by using the constructed QM/MM models were 499 nm (57.3 kcal/mol or 2.48 eV) and 345 nm (83.0 kcal/mol or 3.60 eV) respectively. These values are blueshifted by ca. 7 and 5 kcal/mol (0.30 and 0.22 eV), respectively, relative to the observed values (see Figure 1)

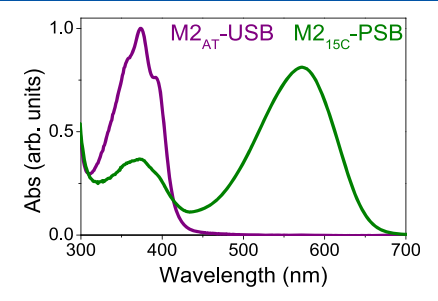


Figure 1. Ground state absorption of the dark adapted $M2_{AT}$ -USB (purple) and light adapted $M2_{15C}$ -PSB (green) states. The $M2_{15C}$ -PSB light state spectrum had contamination of the $M2_{AT}$ -USB dark state as evident by the absorption in the UV region.

and, consistently, the values reported by Borhan, Geiger, and co-workers. 12 These values lie within the reported systematic error (7.5 kcal/mol or 0.33 eV) of the ASEC-FEG protocol which is expected to correctly reproduce trends in λ_{max} rather than in absolute values.²⁵ Furthermore, the visual comparison of computed model against the crystallographic structure indicated that the modeled and observed backbone are substantially consistent with the exception of residues 55-60. As detailed in the Supporting Information, such backbone deviation appears to remove a potentially important π -stacking interaction between a tyrosine residue (TYR59) and the β ionone region of the chromophore. The impact of such removal in our model has been directly tested and found not to significantly modify the vertical excitation energy nor the results of an excited state scan. Accordingly, the constructed models are assumed to be reliable enough for qualitative (i.e., mechanistic) studies reported in the following sections, mainly based on the comparison between experimental and computationally estimated λ_{max} and excited state lifetimes.

 $M2_{ISC}$ -PSB to $M2_{AT}$ -USB Conversion. The 15-cis to all-trans reaction of M2_{15C}-PSB was characterized by using ultrafast transient broadband absorption and cryokinetic spectroscopies. First, the ultrafast pump probe experiment conducted for M2_{15C}-PSB revealed that the decay of the excited state exhibited biphasic decay kinetics with two rate constants (400 fs and 5 ps; see Figure 2A). In the transient absorption spectra (Figure 2B) there is a negative signal between 575 and 625 nm that was ascribed to a ground state bleach given the overlap with the ground state absorption (GSA) and positive excited state absorption (ESA) at 475 nm. There also appears to be a longer-lived negative signal observed (compared to neighboring wavelength such as 650 nm) at 710 nm (Figure S9) and attributed to stimulated emission since it did not follow the GSA band (Figure 2B). The excited state decayed on two different time scales, where the majority (70%) of the excited state population decayed on a 400 fs time scale and a minority (30%) decayed on a 5 ps time scale (Figure 2C,D). The ES population appears to relax back to the ground state, with no measurable long-lived photoproduct, which points to a low quantum efficiency of the reaction.

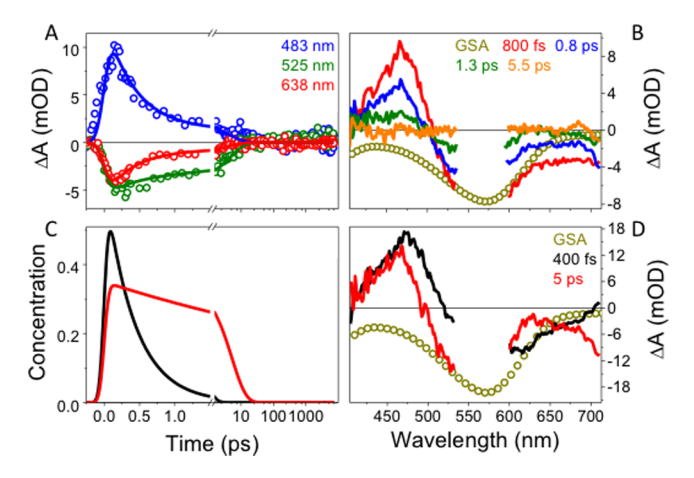


Figure 2. Photodynamics of M2_{1SC}-PSB after 565 nm excitation (A, B). In the kinetics (A), the data are represented by open circles and the fit is represented by solid lines. Global analysis of the same reaction using a parallel model where 70% of the population is in the faster state (C, D). GSA stands for ground state absorption and are represented by open golden circles. The resulting concentration profiles and EADS are color coded to the legend in (D).

The ultrafast studies were complemented with cryokinetic UV—vis spectroscopy as described by Mix et al., ²⁷ which resolved four distinct positive bands (Figure 3, Figures S6—S8,

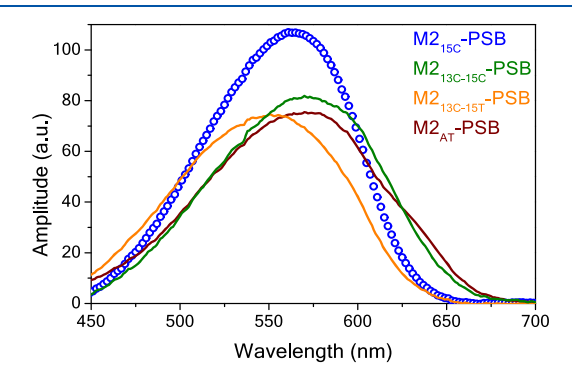


Figure 3. Species associated spectra (SAS) of the PSB intermediates obtained from adding the $M2_{15C}$ -PSB bleach (at the same temperature) to the difference spectra (Figure S6). The $M2_{15C}$ -PSB light state static spectra (blue curve) was taken from the 170 K reference spectra, and $M2_{13C-15C}$ -PSB, $M2_{13C-15T}$ -PSB, and $M2_{AT}$ -PSB photointermediates were isolated at 190, 220, and 240 K, respectively.

Table S1). The first cryotrapped intermediate (M2_{13C-15C}-PSB) was characterized by a red-shifted absorption compared to the parental M2_{15C}-PSB absorption at 560 nm. It was stable to ~180 K whereby it evolves into a second intermediate (M2_{13C-15T}-PSB), which peaks at ~550 nm. This intermediate is stable to ~220 K whereby it then evolves into the next intermediate (M2_{AT}-PSB), which absorbed at an even lower energy of 574 nm. M2_{AT}-PSB persists to ~240 K before evolving into the terminal state peaking at 340 nm, which strongly resembles the ground state M2_{AT}-USB state (Figure S6). This final evolution step is ascribed to a proton transfer event that deprotonates the Schiff base of the chromophore and is responsible for the strong shift in the absorption spectrum from 574 to 340 nm. For these three intermediates, the ground state bleach was added to the difference spectra to produce species associated spectra (SAS) of the photointermediates (Figure 3).

The simulation of the photoinduced dynamics of M2_{15C}-PSB at room temperature as the first step of the M2_{15C}-PSB to M2_{AT}-USB branch of the M2 photocycle is performed by randomly selected 20 initial conditions out of the generated 100 used to simulate the absorption band (see Figure 1 and Figure S1B). Such initial conditions (see Figure S1A) were employed to propagate 20 trajectories starting from S_1 or S_2 (depending from the state displaying the larger initial oscillator strength and therefore transition probability). Within 0.8 ps, seven M2_{15C}-PSB trajectories displayed isomerization and hopped to S₀ while the remaining trajectories remained significantly untwisted. Remarkably, none of the hopped trajectories isomerized around C15=N bond but instead five of them displayed C13=C14 twisting while the remaining two displayed C11=C12 twisting. Both trajectories that exhibited C11=C12 twisting formed, upon S₀ relaxation, the M2_{15C}-PSB reactant and were therefore unproductive. However, the majority of trajectories that isomerized at C13=C14 formed 13-cis,15-cis photoproduct. This is assigned to the first cryogenically trapped M2_{13C-15C}-PSB and is thus called by the same acronym.

All isomerizing trajectories followed the ABP isomerization mechanism similar to that of a natural microbial rhodopsin such as bacteriorhodopsin. In fact, the isomerization around C12—C13=C14—C15 and C14—C15=N—C ε dihedrals takes place concertedly in opposite directions. As illustrated in Figure 4, the twisting of C13=C14 and C15=N increases

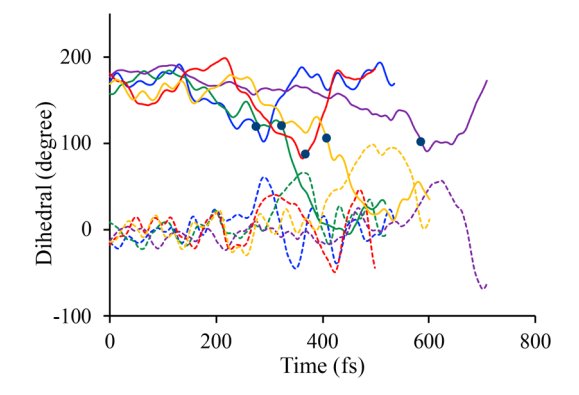


Figure 4. Evolution of C12—C13=C14—C15 (solid) and C14—C15=N—C ε (dashed) dihedrals of the trajectories that displayed isomerization around C13=C14 double bond. Black spheres denote the hop times.

along the trajectories until the molecule hops to the ground state. Once the hop takes place, the C13=C14 twisting continues while the C14—C15=N—C ε dihedral reverts, yielding a net C13=C14 isomerization and, therefore, the above-mentioned M2_{13C-15C}-PSB intermediate (also see Supporting Information for a movie of a representative reactive trajectory).

Since the above trajectory simulations indicate that M2_{1SC}-PSB isomerizes around the C13—C14 double bond leading to the 13-cis,15-cis photoproduct we hypothesize, on the basis of the cryogenic data discussed above, that M2_{1SC}-PSB to M2_{AT}-USB conversion takes place through at least two extra intermediates associated with a single chromophore change each. The second intermediate is predicted to be the 13-cis,15-trans chromophore isomer and is therefore called M2_{13C-15T}-PSB for consistency with the cryogenic assignment. The third intermediate would feature a 13-trans,15-trans chromophore

and it is called M2_{AT}-PSB being assigned to the third cryogenic intermediate. QM/MM models for each intermediate were constructed by using the ASEC-FEG protocol,²⁵ leading to a prediction of their λ_{\max} values. When looking at these values, we concluded that the increased discrepancy from the experimental value of the corresponding cryogenically trapped intermediate reflects the "distance" of the model from the initial X-ray crystallographic structure of M2_{15C}-PSB (the only available template). In particular, while the primary photoproduct M2_{13C-15C}-PSB displays a value close to the experiment, the more distant M2_{13C-15C}-PSB and M2_{AT}-PSB models deviate significantly, suggesting a shortcoming with the modeling. This decrease in model accuracy can be tentatively attributed to the distant template structure. In fact, while the model of the first intermediate is constructed starting from a model constructed on the basis of an X-ray crystallographic structure, the model of the second intermediate is constructed by taking as a template the model of the first intermediate and it is thus not directly related to an experimental structure. Since the model of the third intermediate is constructed from the model of the second, the accuracy issue is further amplified. For this reason, the M2_{13C-15C}-PSB and M2_{AT}-PSB models are not considered in the following discussion.

Given the results of the cryokinetics and of the computation, we propose the scheme reported in Figure 5 for the M2_{15C}-PSB

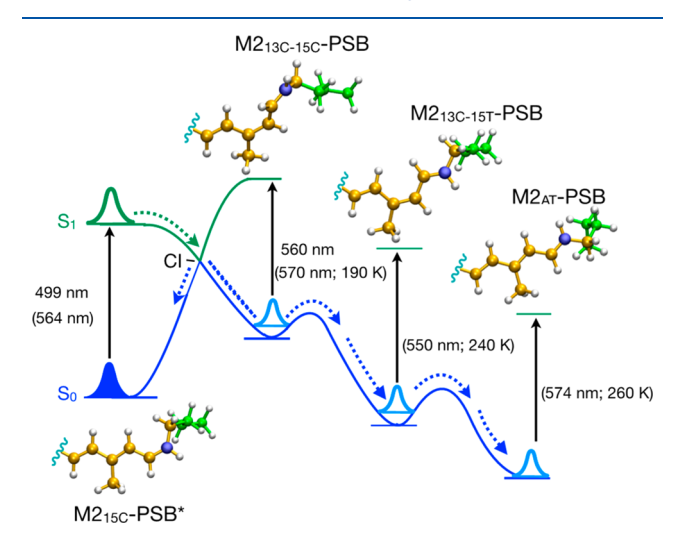


Figure 5. Schematic representation of the PESs driving $M2_{15C}$ -PSB to $M2_{AT}$ -USB conversion. A population of $M2_{15C}$ -PSB molecules absorbing green light is promoted to S_1 . The excited population then relaxes and passes a CI. A fraction of this population reaches the photoproduct form $M2_{13C-15C}$ -PSB. We hypothesize that this subpopulation is further isomerized into $M2_{13C-15T}$ -PSB form and, finally, into $M2_{AT}$ -PSB. The last form undergoes a proton transfer resulting in $M2_{AT}$ -USB. Values in brackets are from the species associated spectra (Figure 3) from the cryokinetics experiments. * denotes a model constructed from crystallographic structure. PDB ID: 4YFP.

to $M2_{AT}$ -USB part of the M2 photocycle. The structure of the chromophore in $M2_{13C-15C}$ -PSB and $M2_{AT}$ -PSB is hypothetical and just follows the shortest possible sequential isomerization path from $M2_{13C-15C}$ -PSB to $M2_{AT}$ -PSB, again considering sequential single chemical changes in the chromophore.

Comparison of computed and observed excited state lifetimes (400 ps from ultrafast measurements and theory; Figures 2 and 4) and the λ_{max} values (Figures 3 and 5) suggests

that our description of the primary event is qualitatively correct. More specifically, the red shifting of the computationally predicted first intermediate agrees with the experimentally observed spectral trend, where the initial photointermediate absorption is red-shifted with respect to the reactant absorption. The cryogenic data are then consistent with a blue-shifted secondary intermediate and a red-shifted tertiary intermediate, before blue-shifting to the $M2_{\rm AT}$ -USB dark state.

 $M2_{AT}$ -USB to $M2_{ISC}$ -PSB Conversion. As with $M2_{ISC}$ -PSB dynamics, the dynamics of $M2_{AT}$ -USB was characterized by ultrafast and cryokinetics experiments. The ultrafast transient absorption spectra and kinetics of $M2_{AT}$ -USB are displayed in Figure 6, where the primary observation is the decay of the

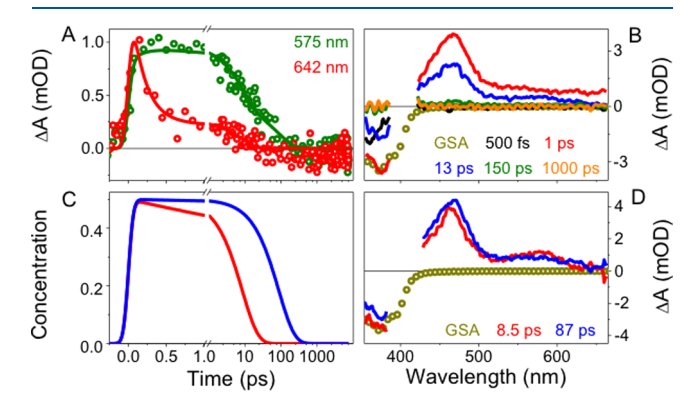


Figure 6. Photodynamics (aof $M2_{AT}$ -USB after 400 nm excitation (A, B). The fits (A, solid lines) are the results of a parallel model consisting of two populations with equal contribution. Concentration and EADS (C, D) from the fit are color coded to the legend in (D). No photoproduct is resolved and only two excited state populations with characteristic double peak features are observed.

excited state back to the ground state over 750 ps. In addition to the decay of the excited state, an evolution of a negative signal in the 575-642 nm (Figure 6A) region over ~ 300 ps is observed, but due to the location and broadness of the signal this is attributed to PSB contamination. In addition to the appearance of the negative signal for the 642 nm trace (Figure 6A, red curve), there is also a short-lived (c.a. < 200 fs) positive peak that spans from ~ 625 from 650 nm and is attributed to an early time artifact. The ultrafast data set was fit with a parallel model, and the resulting concentration profile and EADS are depicted in Figure 6C,D, where the red and blue curves represent excited state absorption decay back to the ground state.

The cryokinetics resolved a population red shifted of M2_{AT}-USB and was attributed to M2_{15C}-PSB (Figures 7, S10–S12, and Table S2). M2_{15C}-USB decays back into M2_{AT}-USB at 180 and 190 K, suggesting the presence of a shunt back to M2_{AT}-USB (Figure S10E ,H) and directly evolves into the M2_{15C}-PSB photoproduct between 210 and 230 K (Figure S11G–I). When a high enough temperature (240 K) was reached, a decay of the green absorbing band and a filling of the GSB was observed, suggesting dark conversion back to M2_{AT}-USB (Figures S11 and S12). This shows that M2_{AT}-USB evolves to M2_{15C}-PSB through a single intermediate that is followed by a protonation to the photoproduct. The M2_{15C}-USB photointermediate was not observed in the room temperature dynamics due to the low quantum efficiency of its formation. The M2_{15C}-PSB photoproduct is thermally stable up to 240 K

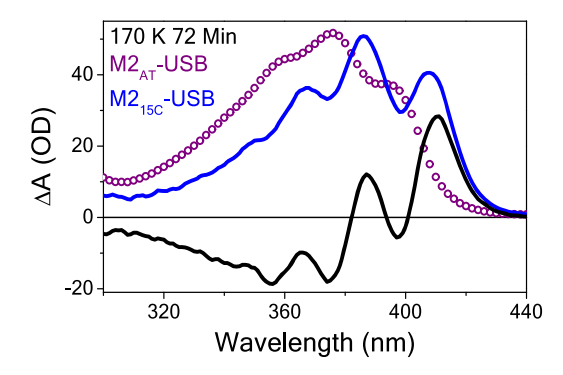


Figure 7. $M2_{AT}$ -USB dark state static spectra (purple open circles curve), difference spectra (black curve), and species associated spectra (SAS; blue curve) of the $M2_{15C}$ -USB intermediate at 170 K. The SAS was obtained from adding the $M2_{AT}$ -USB bleach to the difference spectra.

where it thermally reconverts back to the deprotonated $M2_{AT}$ -USB.

In addition to the experimental results, the photoinduced dynamics of the $M2_{AT}$ -USB to $M2_{1SC}$ -PSB branch of the M2 photocycle were studied by initiating $M2_{AT}$ -USB trajectories on S_3 or S_4 at the 5-root-state-average CASSCF level due to their high oscillator strength. During the 0.8 ps simulation time, the majority of the trajectories hopped to S_3 or S_2 states but displayed no sign of isomerization possibly due to an encountered small barrier. For this reason, we then mapped the excited state isomerization path driven by the C15=N twist by computing a relaxed scan starting from the $M2_{AT}$ -USB.

At this point, it is important to recall information on two important CIs related to the photoisomerization of conjugated polyene systems. The first is a crossing between two states having $1A_{\rm g}$ and $1B_{\rm u}$ electronic structures ($1B_{\rm u}/1A_{\rm g}$ crossing featuring a single 90° twisted C=C bond) and is found in cationic conjugated systems such as rPSB. The second, a crossing between $2A_{\rm g}$ and $1A_{\rm g}$ like states ($2A_{\rm g}/1A_{\rm g}$ crossing, also called a (CH)₃-kinked CI) is found in nonpolar systems.

Since rUSB is not a highly polar chromophore, we first assumed that a $2A_g/1A_g$ kinked CI, is more stable in comparison to $1B_u/1A_g$ CI and thus more accessible from the Franck-Condon (FC) point. Hence, we mapped the reaction path starting from the FC point and connecting it to a previously optimized 2A_g/1A_g CI. The computed path shows the existence of an S₁ minimum, but it also shows that reaching the CI from the minimum is impossible as this lies \sim 37 kcal/ mol higher (see Figure S13). We then computed similar reaction paths for the isomerization around C11=C12 and C13=C14 double bonds. The results are reported in Figure S14. We then hypothesized that rUSB isomerizes around C15=N and that the reaction proceeds through a 1B_u/1A_o CI that was previously optimized. The computed reaction path is reported in Figure 8. The electronic states are labeled from S₀ to S₅ based on the order of the CASSCF energy at the FC region.

At the FC point, the computed oscillator strength maximum (2.3) corresponds to the $S_0 \rightarrow S_5$ transition at the CASSCF level. With the correction for dynamic electron correlation energy, the S_5 state becomes the lowest excited state at the CASPT2 level. The geometry optimization on S_5 resulted in a minimum whose S_1 and S_5 CASPT2 energy order is switched. This indicates a crossing between the first two lowest excited states at the CASPT2 level. We then proceeded with a S_1

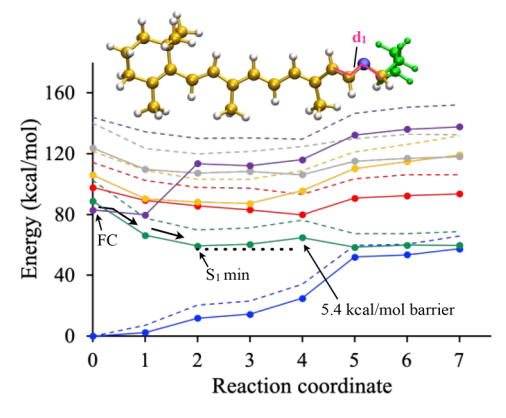


Figure 8. Evolution of CASSCF (dashed) and CASPT2 energies (solid) along the isomerization of $M2_{AT}$ -USB around the C15=N double bond. S_0 to S_5 states are denoted by blue, green, red, yellow, gray, and violet colors, respectively. Points 3–7 of the reaction coordinate were obtained from a series of constraint geometry optimizations. More specifically, the geometry optimizations were carried out while keeping dihedral d_1 (see USB structure on top) constrained at -160, -140, -120, -110, and -90° , respectively.

geometry optimization that resulted in a S_1 minimum located ca. 59 kcal/mol. This is assigned to the primary excited state photoproduct intermediate generated after photon absorption.

At this stage, it is important to mention that the above findings on rUSB isomerization display similarities to the information uncovered from the Siberian hamster cone pigments.³¹ The calculations carried out at the CASPT2// CASSCF/6-31G* level in both studies indicate the following. First, at the FC point, the lowest energy 1B_n-like state turns out to be the spectroscopically most favorable state at the CASPT2 level. Second, there is a crossing between the lowest two excited states (2A_o/1B_u crossing) immediately after relaxation from the FC point. Third, once the molecule passes such a crossing, it may reach a minimum on the lowest excited state; but the molecular structure of such a minimum does not exhibit inverted bond length alternation (BLA), which is essential for the double bond photoisomerization. However, we observe an expansion in the double bonds and a contraction in the single bonds when going from S₀ optimized to S₁ optimized structures (see Figure S15 for geometric parameters). This suggests that there is a barrier along the BLA coordinate. We computed the rest of the reaction path by constraining C14—C15=N—C ε and computing a relaxed scan. The path shows a small ca. 5.4 kcal/mol energy barrier between S_1 minimum and the S_0/S_1 crossing which has a $1B_0/S_1$ 2A_g CI structure.

On the basis of the above information, we propose the mechanistic scheme of Figure 9 for the $M2_{AT}$ -USB to $M2_{1SC}$ -PSB conversion. Note that the calculated excited state barrier (the 5.4 kcal/mol seen in Figure 8; 1.6 ps excited state lifetime from Eyring equation), is consistent with the observed lifetime 8.5 ps (6.4 kcal/mol barrier from Eyring equation; 50% excited state population) excited state lifetime in $M2_{AT}$ -USB ultrafast experiments.

Proposed M2 Photocycle Mechanism. According to the above results and to the assumed shortest possible, single chemical event, sequential isomerization hypothesis mentioned above, the molecular-level motion driving the M2 photocycle changes are proposed as follows (see Figure 10). The M2_{15C}-PSB to M2_{13C-15C}-PSB photoisomerization takes place via an ABP mechanism involving the C13=C14 and C15=N bonds. If

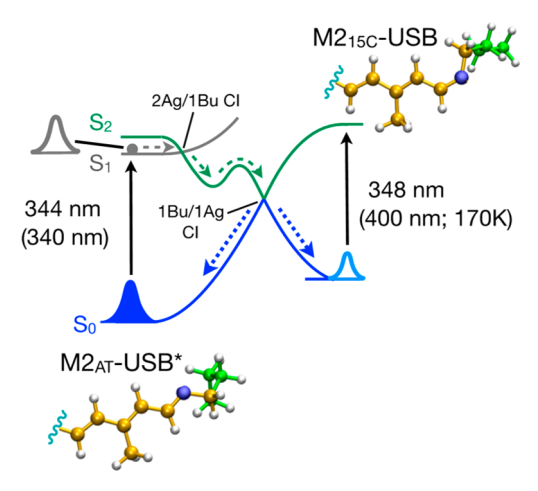


Figure 9. Proposed isomerization pathway for the $M2_{AT}$ -USB to $M2_{15C}$ -PSB conversion. A population of $M2_{AT}$ -USB absorbing a UV light pulse reaches the lowest excited state at the FC region. It is then relaxed on the same state and crossed to the second excited state which is now lower in energy. The population is further relaxed on this state and reaches a minimum and proceeds toward a second CI and reaches the ground state photoproduct. It then undergoes the proton transfer and reaches the $M2_{15C}$ -PSB state. The wavelengths are in nm, and the values reported in parentheses are experimentally reported values extracted from SAS for the $M2_{15C}$ -USB from the cryokinetics (Figure 7). * denotes a model constructed from the crystallographic structure. PDB ID: 4YFQ.

we consider plane β , which is defined by C14, C15, and H15 atoms and looking through the C14-C15 single bond in the direction of the β -ionone ring, the plane rotates in the clockwise direction. This suggests that C13=C14 and C15= N double bonds twist in clockwise and counterclockwise directions, respectively. After the isomerization, a M2_{AT}-PSB intermediate is produced after two thermal steps (see Figure 5) indicated by the experimental investigations. At this stage, the deprotonation of the rPSB takes place. We examined the molecular structures that constitute the M2_{AT}-PSB ASEC configuration and noted a hydrogen bond network connecting the iminium hydrogen and a glutamate (GLU73 residue) located ca. 9 Å away from it. This network is also observed in the structure closest to the average (see Figure S16A). We propose that the proton translocation from rPSB to GLU73 takes place through such a network involving, according to our model, at least three water molecules during the M2_{AT}-PSB to M2_{AT}-USB conversion.

As discussed above, M2_{AT}-USB then undergoes an isomerization around the C15=N bond in the presence of UV light and produces M2_{15C}-USB directly. The corresponding atomic motion can be described similar to the M2_{15C}-PSB case by considering a plane γ defined by C ε , N15, and the nitrogen lone pair. During M2_{AT}-USB isomerization, the C15=N bond continues to twist in the counterclockwise direction while the C13=C14 bond undergoes a slight twist in the clockwise direction. The corresponding photoproduct regenerates the M2_{15C}-PSB by obtaining a proton from the environment. We

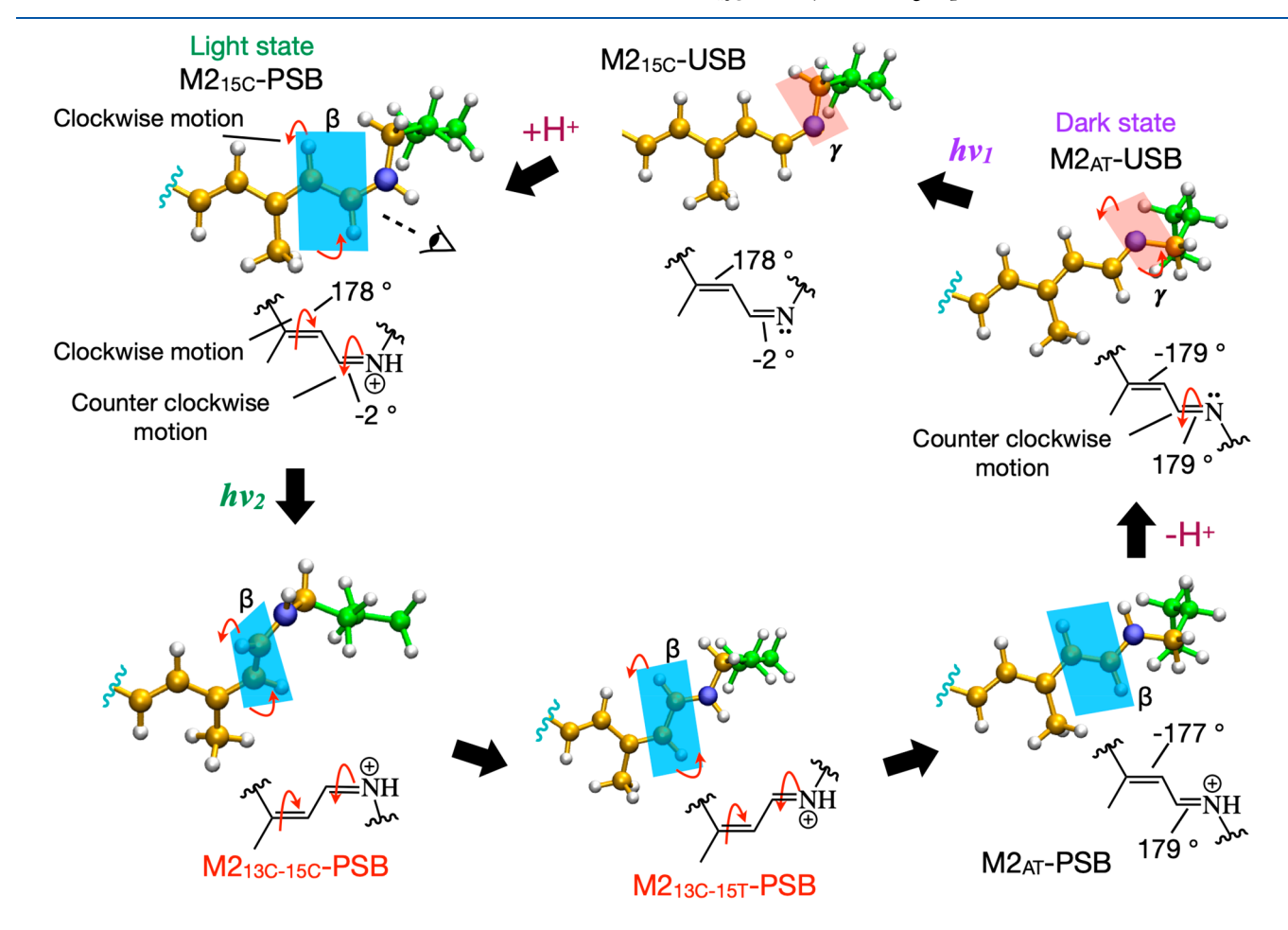


Figure 10. Proposed mechanism for the M2 photocycle. Hypothetical models are labeled in red.

propose that a proton residing on the nearby glutamic acid residue (GLH73) is transferred to the Schiff base in this process. Moreover, we propose that such a transfer occurs through a H bond network that involves at least one water molecule (see Figure S16B).

Is M2 a Good Model System To Study the Factors Effecting Rhodopsin Photoisomerization? The features of M2 that we have discussed above, especially in its rPSB bound form, are not too far from the isomerization of certain microbial rhodopsins. These include (1) the primary photoisomerization of the rPSB occurring at the C13=C14 double bond, (2) the isomerization intermediates bearing similarities to the ones proposed and documented for Anabaena sensory rhodopsin, 32,33 (3) the presence on an ABP photoisomerization mechanism which has been shown in bacteriorhodopsin. 11,34 We have also uncovered a fourth feature of this system, namely, electronic state mixing, that we have previously documented for animal and microbial rhodopsin and rPSB in solution (see section S9).²⁹ The fact that M2_{15C}-PSB photoisomerization is similar to natural rhodopsins is, in many ways, an indication that it may be used as a model system to study the chromophore/protein interaction governing rhodopsin photocycles.

In conclusion, above we have studied the photocycle of a man-made rhodopsin, M2, that can undergo reversible photoisomerization. The study has been carried out with a combination of theory and experiments. The results suggest that the photocycle involves several intermediates and two separate photoisomerization events that are initiated by the absorption of photons with very different wavelengths. More specifically, green light excites M2_{15C}-PSB, which produces 13cis,15-cis photoproduct which then isomerizes into 13-cis,15trans and, finally, an all-trans form. This process is associated with the ABP photoisomerization mechanism, which has never been documented in an artificial rhodopsin before. Our results also reinforce the idea that the bicycle-pedal isomerization mechanism does not necessarily occur inside a space confining environment and can be rather an intrinsic property of the chromophore.35,36

The photoisomerization of rUSB takes place directly around the C15—N double bond from 15-trans into 15-cis form. The consistency between our findings related to rUSB isomerization and Siberian hamster cone pigments suggests that the information we have documented above may be valid for other rhodopsins hosting rUSB chromophores. For instance, such information may be useful to investigate the UV pigments found in birds and fish.³⁷

The observation that while a PSB gives a 13-cis photoproduct, the rUSB gives rise to photoisomerization of the C15—N bond is consistent with a recent study of a rhodopsin mimic variant of M2.³⁸ In this study, it was shown that an all-trans retinylidene can be photoisomerized to a stable 13-cis,15-cis product; but only in its PSB state. This illustrates the clear difference in photoproduct outcome between protonated and unprotonated systems, as predicted here. The production of the 13-cis,15-cis photoproduct suggests a similar ABP photoisomerization mechanism in this rhodopsin mimic as well.

ASSOCIATED CONTENT

Supporting Information

The Supporting Information is available free of charge at https://pubs.acs.org/doi/10.1021/acs.jpclett.0c00751.

Computational methods, distribution of the absorption energies and computed absorption bands, ASEC protocol diagram, QM/MM setup, schematic of flow of an average cryokinetics experiment, energy profiles, cryokinetic difference spectra, cryokinetic spectra, kinetics, EADS, extracted dynamics, geometric parameters, proton transfer mechanisms, tables of observations and interpretations (PDF)

M2_{15C}-PSB isomerization (AVI)

AUTHOR INFORMATION

Corresponding Authors

Babak Borhan — Department of Chemistry, Michigan State University, Lansing, Michigan 48824, United States;

orcid.org/0000-0002-3193-0732; Email: babak@chemistry.msu.edu

James H. Geiger – Department of Chemistry, Michigan State University, Lansing, Michigan 48824, United States; Email: geiger@chemistry.msu.edu

Delmar S. Larsen — Department of Chemistry, University of California, Davis, Davis, California 95616, United States; orcid.org/0000-0003-4522-2689; Email: dlarsen@ucdavis.edu

Massimo Olivucci — Department of Chemistry, Bowling Green State University, Bowling Green, Ohio 43403, United States; Dipartimento di Biotecnologie, Chimica e Farmacia, Università di Siena, I-53100 Siena, Italy; Institut de Physique et Chimie des Maferiaux de Strasbourg, UMR 7504 Université de Strasbourg-CNRS, F-67034 Strasbourg, France; oocid.org/0000-0002-8247-209X; Email: molivuc@bgsu.edu, olivucci@unisi.it

Authors

Madushanka Manathunga — Department of Chemistry, Bowling Green State University, Bowling Green, Ohio 43403, United States; Oorcid.org/0000-0002-3594-8112

Adam J. Jenkins – Department of Chemistry, University of California, Davis, Davis, California 95616, United States

Yoelvis Orozco-Gonzalez — Department of Chemistry, Bowling Green State University, Bowling Green, Ohio 43403, United States; ♥ orcid.org/0000-0001-7225-2424

Alireza Ghanbarpour — Department of Chemistry, Michigan State University, Lansing, Michigan 48824, United States;
orcid.org/0000-0002-7485-029X

Complete contact information is available at: https://pubs.acs.org/10.1021/acs.jpclett.0c00751

Notes

The authors declare no competing financial interest.

ACKNOWLEDGMENTS

This work was supported in part by the Italian MIUR for funding (PRIN 2015) and, in part, by the National Science Foundation under grants no. CHE-1710191 and CHE-1413739 and National Institute of Health under grant no. R15GM126627. M.O. is grateful to the Ohio Supercomputer Center for granted computer time. Dr. Jack Fuzell is acknowledged for assistance in the initial setting up of the M2_{AT}-PSB cryokinetics and Dr. L Tyler Mix is acknowledged for consultation on ultrafast data collection and fitting. Dr. Mikas Vengris is also acknowledged for donating the global and target analysis software.

REFERENCES

- (1) Spudich, J. L.; Yang, C. S.; Jung, K. H.; Spudich, E. N. Retinylidene Proteins: Structures and Functions from Archaea to Humans. *Annu. Rev. Cell Dev. Biol.* **2000**, *16*, 365–392.
- (2) Kandori, H.; Shichida, Y.; Yoshizawa, T. Photoisomerization in Rhodopsin. *Biochemistry* **2001**, *66*, 1197–1209.
- (3) Ernst, O. P.; Lodowski, D. T.; Elstner, M.; Hegemann, P.; Brown, L. S.; Kandori, H. Microbial and Animal Rhodopsins: Structures, Functions, and Molecular Mechanisms. *Chem. Rev.* **2014**, *114*, 126–163.
- (4) Schoenlein, R. W.; Peteanu, L. A.; Mathies, R. A.; Shank, C. V. The First Step in Vision: Femtosecond Isomerization of Rhodopsin. *Science* **1991**, 254, 412–415.
- (5) Peteanu, L. A.; Schoenlein, R. W.; Wang, Q.; Mathies, R. A.; Shank, C. V. The First Step in Vision Occurs in Femtoseconds: Complete Blue and Red Spectral Studies. *Proc. Natl. Acad. Sci. U. S. A.* 1993, 90, 11762–11766.
- (6) Kim, J. E.; Tauber, M. J.; Mathies, R. A. Wavelength Dependent Cis-Trans Isomerization in Vision. *Biochemistry* **2001**, *40*, 13774–13778.
- (7) Warshel, A. Bicycle-Pedal Model for the First Step in the Vision Process. *Nature* **1976**, *260*, *679*–*683*.
- (8) Warshel, A.; Chu, Z. T.; Hwang, J.-K. The Dynamics of the Primary Event in Rhodopsins Revisited. *Chem. Phys.* **1991**, *158*, 303–314
- (9) Dormans, G. J. M.; Groenenboom, G. C.; Van Dorst, W. C. A.; Buck, H. M. A Quantum Chemical Study on the Mechanism of Cis-Trans Isomerization in Retinal-like Protonated Schiff Bases. *J. Am. Chem. Soc.* **1988**, *110*, 1406–1415.
- (10) Warshel, A.; Barboy, N. Energy Storage and Reaction Pathways in the First Step of the Vision Process. *J. Am. Chem. Soc.* **1982**, *104*, 1469–1476.
- (11) Yu, J. K.; Liang, R.; Liu, F.; Martínez, T. J. First-Principles Characterization of the Elusive I Fluorescent State and the Structural Evolution of Retinal Protonated Schiff Base in Bacteriorhodopsin. J. Am. Chem. Soc. 2019, 141, 18193—18203.
- (12) Nosrati, M.; Berbasova, T.; Vasileiou, C.; Borhan, B.; Geiger, J. H. A Photoisomerizing Rhodopsin Mimic Observed at Atomic Resolution. *J. Am. Chem. Soc.* **2016**, *138*, 8802–8808.
- (13) Crist, R. M.; Vasileiou, C.; Rabago-Smith, M.; Geiger, J. H.; Borhan, B. Engineering a Rhodopsin Protein Mimic. *J. Am. Chem. Soc.* **2006**, *128*, 4522–4523.
- (14) Berbasova, T.; Santos, E. M.; Nosrati, M.; Vasileiou, C.; Geiger, J. H.; Borhan, B. Light-Activated Reversible Imine Isomerization: Towards a Photochromic Protein Switch. *ChemBioChem* **2016**, *17*, 407–414.
- (15) Schapiro, I.; Ruhman, S. Ultrafast Photochemistry of Anabaena Sensory Rhodopsin: Experiment and Theory. *Biochim. Biophys. Acta, Bioenerg.* **2014**, *1837*, 589–597.
- (16) Matsuyama, T.; Yamashita, T.; Imamoto, Y.; Shichida, Y. Photochemical Properties of Mammalian Melanopsin. *Biochemistry* **2012**, *51*, 5454–5462.
- (17) Ehrenberg, D.; Varma, N.; Deupi, X.; Koyanagi, M.; Terakita, A.; Schertler, G. F. X.; Heberle, J.; Lesca, E. The Two-Photon Reversible Reaction of the Bistable Jumping Spider Rhodopsin-1. *Biophys. J.* **2019**, *116*, 1248–1258.
- (18) Melloni, A.; Rossi Paccani, R.; Donati, D.; Zanirato, V.; Sinicropi, A.; Parisi, M. L.; Martin, E.; Ryazantsev, M.; Ding, W. J.; Frutos, L. M.; et al. Modeling, Preparation, and Characterization of a Dipole Moment Switch Driven by Z/E Photoisomerization. *J. Am. Chem. Soc.* **2010**, *132*, 9310–9319.
- (19) Gozem, S.; Melaccio, F.; Luk, H. L.; Rinaldi, S.; Olivucci, M. Learning from Photobiology How to Design Molecular Devices Using a Computer. *Chem. Soc. Rev.* **2014**, *43*, 4019–4036.
- (20) Sinicropi, A.; Martin, E.; Ryazantsev, M.; Helbing, J.; Briand, J.; Sharma, D.; Leonard, J.; Haacke, S.; Cannizzo, A.; Chergui, M.; et al. An Artificial Molecular Switch That Mimics the Visual Pigment and Completes Its Photocycle in Picoseconds. *Proc. Natl. Acad. Sci. U. S. A.* 2008, 105, 17642–17647.

- (21) Gueye, M.; Manathunga, M.; Agathangelou, D.; Orozco, Y.; Paolino, M.; Fusi, S.; Haacke, S.; Olivucci, M.; Léonard, J. Engineering the Vibrational Coherence of Vision into a Synthetic Molecular Device. *Nat. Commun.* **2018**, *9*, 313.
- (22) McIsaac, R. S.; Bedbrook, C. N.; Arnold, F. H. Recent Advances in Engineering Microbial Rhodopsins for Optogenetics. *Curr. Opin. Struct. Biol.* **2015**, 33, 8–15.
- (23) Huntress, M. M.; Gozem, S.; Malley, K. R.; Jailaubekov, A. E.; Vasileiou, C.; Vengris, M.; Geiger, J. H.; Borhan, B.; Schapiro, I.; Larsen, D. S.; et al. Toward an Understanding of the Retinal Chromophore in Rhodopsin Mimics. *J. Phys. Chem. B* **2013**, *117*, 10053–10070.
- (24) Frutos, L. M.; Andruniów, T.; Santoro, F.; Ferré, N.; Olivucci, M. Tracking the Excited-State Time Evolution of the Visual Pigment with Multiconfigurational Quantum Chemistry. *Proc. Natl. Acad. Sci. U. S. A.* **2007**, *104*, 7764–7769.
- (25) Orozco-Gonzalez, Y.; Manathunga, M.; Marín, M. D. C.; Agathangelou, D.; Jung, K. H.; Melaccio, F.; Ferré, N.; Haacke, S.; Coutinho, K.; Canuto, S.; et al. An Average Solvent Electrostatic Configuration Protocol for QM/MM Free Energy Optimization: Implementation and Application to Rhodopsin Systems. *J. Chem. Theory Comput.* **2017**, *13*, 6391–6404.
- (26) Carroll, E. C.; Compton, O. C.; Madsen, D.; Osterloh, F. E.; Larsen, D. S. Ultrafast Carrier Dynamics in Exfoliated and Functionalized Calcium Niobate Nanosheets in Water and Methanol. *J. Phys. Chem. C* **2008**, *112*, 2394–2403.
- (27) Mix, L. T.; Kirpich, J.; Kumauchi, M.; Ren, J.; Vengris, M.; Hoff, W. D.; Larsen, D. S. Bifurcation in the Ultrafast Dynamics of the Photoactive Yellow Proteins from Leptospira Biflexa and Halorhodospira Halophila. *Biochemistry* **2016**, *55*, 6138–6149.
- (28) Gozem, S.; Luk, H. L.; Schapiro, I.; Olivucci, M. Theory and Simulation of the Ultrafast Double-Bond Isomerization of Biological Chromophores. *Chem. Rev.* **2017**, *117*, 13502–13565.
- (29) Manathunga, M.; Yang, X.; Orozco-Gonzalez, Y.; Olivucci, M. Impact of Electronic State Mixing on the Photoisomerization Time Scale of the Retinal Chromophore. *J. Phys. Chem. Lett.* **2017**, *8*, 5222.
- (30) Sampedro Ruiz, D.; Cembran, A.; Garavelli, M.; Olivucci, M.; Fuß, W. Structure of the Conical Intersections Driving the Cis-Trans Photoisomerization of Conjugated Molecules. *Photochem. Photobiol.* **2002**, *76*, 622–633.
- (31) Bonvicini, A.; Demoulin, B.; Altavilla, S. F.; Nenov, A.; El-Tahawy, M. M. T.; Segarra-Martí, J.; Giussani, A.; Batista, V. S.; Garavelli, M.; Rivalta, I. Ultraviolet Vision: Photophysical Properties of the Unprotonated Retinyl Schiff Base in the Siberian Hamster Cone Pigment. *Theor. Chem. Acc.* **2016**, *135*, 110.
- (32) Strambi, A.; Durbeej, B.; Ferré, N.; Olivucci, M. Anabaena Sensory Rhodopsin Is a Light-Driven Unidirectional Rotor. *Proc. Natl. Acad. Sci. U. S. A.* **2010**, *107*, 21322–21326.
- (33) Kawanabe, A.; Furutani, Y.; Jung, K.-H.; Kandori, H. Photochromism of Anabaena Sensory Rhodopsin. *J. Am. Chem. Soc.* **2007**, *129*, 8644–8649.
- (34) Altoè, P.; Cembran, A.; Olivucci, M.; Garavelli, M. Aborted Double Bicycle-Pedal Isomerization with Hydrogen Bond Breaking Is the Primary Event of Bacteriorhodopsin Proton Pumping. *Proc. Natl. Acad. Sci. U. S. A.* **2010**, *107*, 20172–20177.
- (35) Schapiro, I.; Weingart, O.; Buss, V. Bicycle-Pedal Isomerization in a Rhodopsin Chromophore Model. *J. Am. Chem. Soc.* **2009**, *131*, 16–17.
- (36) Weingart, O. The Twisted C11C12 Bond of the Rhodopsin ChromophoreA Photochemical Hot Spot. *J. Am. Chem. Soc.* **2007**, 129, 10618–10619.
- (37) Jacobs, G. H. Ultraviolet Vision in Vertebrates. *Am. Zool.* **1992**, 32, 544–554.
- (38) Ghanbarpour, A.; Nairat, M.; Nosrati, M.; Santos, E. M.; Vasileiou, C.; Dantus, M.; Borhan, B.; Geiger, J. H. Mimicking Microbial Rhodopsin Isomerization in a Single Crystal. *J. Am. Chem. Soc.* **2019**, *141*, 1735–1741.